MR Image Reconstruction using Densely Connected Residual Convolutional Networks

Amir Aghabiglou[a], Ender M. Eksioglu[b,*]

[a] *Graduate School, Istanbul Technical University, Istanbul, Turkey*
[b] *Electronics and Communication Engineering Department, Istanbul Technical University, Istanbul, Turkey*

Abstract

MR image reconstruction techniques based on deep learning have shown their capacity for reducing MRI acquisition time and performance improvement compared to analytical methods. Despite the many challenges in training these rather large networks, novel methodologies have enhanced the capability for having clinical-grade MR image reconstruction in real-time. In recent literature, novel developments have facilitated the utilization of deep networks in various image processing inverse problems. In particular, it has been reported multiple times that the performance of deep networks can be improved by using short connections between layers. In this study, we introduce a novel MRI reconstruction method that utilizes such short connections. The dense connections are used inside densely connected residual blocks. Inside these blocks, the feature maps are concatenated to the subsequent layers. In this way, the extracted information is propagated until the last stage of the block. We have evaluated this densely connected residual block's efficiency

*Corresponding author

Email addresses: `aghabaiglou17@itu.edu.tr` (Amir Aghabiglou), `eksioglue@itu.edu.tr` (Ender M. Eksioglu)

in MRI reconstruction settings, by augmenting different types of effective deep network models with these blocks in novel structures. The quantitative and qualitative results indicate that this original introduction of the densely connected blocks to the MR image reconstruction problem improves the reconstruction performance significantly.

Keywords: Magnetic resonance imaging, Image reconstruction, Deep learning, DCR blocks

---

1. Introduction

Magnetic resonance imaging (MRI) is a widely used non-invasive medical imaging technique [1]. However, despite its popularity and advantages, the required data acquisition and image formation process is a rather lengthy operation. During this reconstruction procedure, patients need to be motionless in order to acquire high-quality images without artifacts. MRI data are acquired in the k-space, and the data acquisition process necessitates a tradeoff between reconstruction quality and reconstruction time. As a possible solution to this tradeoff, various MRI acceleration methods using compressed sensing (CS) [2, 3] and deep learning (DL) have been introduced. These pipelines have led to both faster and better reconstruction of MR images from reduced (undersampled) k-space data acquired in the Fourier domain. As another example, in [4] high-quality MR images were reconstructed from initial low-resolution images in two steps. The MR image blurring effects (originating from the initial super-resolution step) were lessened in a sparse derivative prior process. In other studies, CS-MRI models were developed by employing the plug-and-play framework [5], where image denoising is directly utilized as a regularization prior [6, 7]. In these particular works, the block matching 3D (BM3D) denoiser is employed to reconstruct MR images by using a sparsity prior technique. However, the iterative CS-MRI methods are rather slow, and they also suffer from high computational costs because of the iterative optimization solutions. Hence, deep learning-based solutions for MRI reconstruction have experienced a great surge in the recent literature [8, 9, 10].

Lately, deep learning-based methods have received attention as a means of accelerating MRI reconstruction. In this regard, some novel deep learning techniques from image processing and computer vision have been applied to this problem. One important example of these successful deep learning methods utilizes domain-transform manifold learning [11]. In this work, automated transform by manifold approximation (AUTOMAP) [11] is adapted to the MRI reconstruction problem using data-driven learning. In another paper, a variational reconstruction network is developed, and it is applied in particular to knee image reconstruction [12]. Among various deep learning models, the U-Net algorithm has gained noticeable success in diverse fields of image processing. Initially, the U-Net [13] had been suggested as an image segmentation framework. However, it has found its way in other image processing inverse problems, including MR image reconstruction. The superiority of the U-Net is attributed to its capability in extracting features with different scales using upsampling (decoder) and downsampling (encoder) stages.

In [14] an encoder-decoder model has been provided for compressed sensing MR image reconstruction. The model has been evaluated using two different datasets. In another study, a wide multimodal U-Net [15] has been proposed for accelerating MRI reconstruction by working on the k-space data in the feed-forward path of encoding. Better perceptual quality has been gained by using this method. In [16], a deep residual U-Net is trained in the k-space domain to reduce the aliasing artifacts. In [17], Hyun et al. provided an improved U-Net based structure by applying a correction step in the k-space.

An increase in the number of convolutional layers and consequent deepening of networks leads to performance improvement. However, due to the concurrent amplification of the number of parameters, the network becomes more susceptible to gradient loss, and the training procedure becomes prone to failure. Vanishing gradients during the training step hampers the parameter update in the backpropagation procedure [18]. The quest for deeper but still trainable networks motivated researchers to develop designs with an increased number of connections through the use of unrolled solutions, e.g. the cascade network of [19] for MRI reconstruction. As another approach for the solution of the vanishing gradients problem, in [20] dense connections through densely connected blocks were introduced in the DenseNet setting. This block has found its way to other image processing problems. A hierarchical densely connected network was developed for image denoising in [21]. Converting the model to a hierarchical framework mitigates the memory consumption and alleviates the computational burden. In [22], DenseNet and ResNet were combined leading to the Residual Dense Network and densely connected residual blocks (DCRs). In another recent work, DenseNets have been used for segmentation problems using the encoder-decoder network [23]. In this work, the convolutional neural network in both the downsampling and upsampling stage has been replaced with DenseNets [23]. In yet another study, the dense connection was tested for a super-resolution problem in MRI [24]. In [25] on the other hand, convolutional layers were reused through a super-resolution CNN with dense skip connection.

Encouraged by these successful applications of dense connections, here we are leveraging the use of DCR blocks to the MRI reconstruction problem by using them inside residual convolutional neural networks (CNNs) and encoder-decoder type U-Nets. To the best of our knowledge, this forms the first use of DCR blocks in MR image reconstruction applications. The application of DCR blocks enables us to make the network deeper and to increase the number of model parameters without the consequent training difficulties and vanishing gradient problems. The extracted feature maps in each step are carried to the following convolutional layers by successive concatenation operations. The qualitative and quantitative results point out that the reconstruction performance of the DCR infused deep networks are considerably enhanced when compared to their original counterparts.

The rest of this paper is arranged as follows. In the second section, we detail the novel MRI reconstruction framework utilizing the densely connected DCR blocks. Afterward, we review the particular network structures introduced through the developed DCR framework. In the next step, the utilized dataset and the experimental setup details are provided. The third section reports the quantitative and qualitative results of reconstructed images, including the results for the novel structures and also structured from

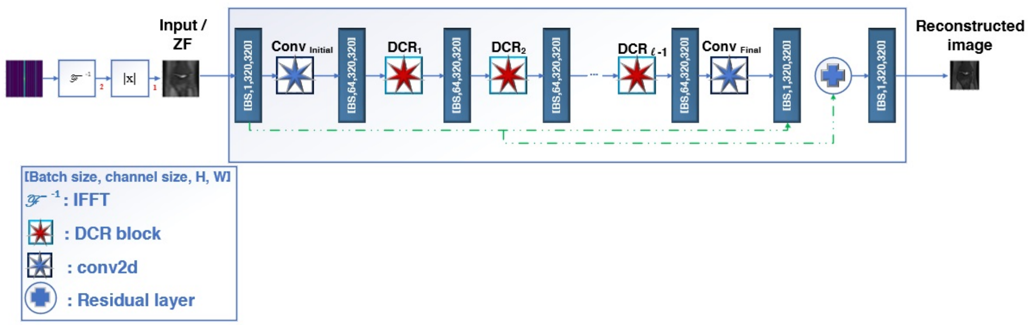

Figure 1: Densely Connected Residual CNN with L layers.

the literature. Moreover, in this section we highlighted the statistical significance and difference of proposed models regarding the state-of-the-art models in MR image reconstruction. Finally in the last part, the conclusions are stated.

2. Method

2.1. Densely connected residual network in MR image reconstruction

In our proposed framework (as detailed in Figs.1 and 2), a single channel zero-filling (ZF) image is fed as input into a convolutional neural network with L layers. The network includes non-linear convolutional layers indicated by the operator $\mathscr{F}_{\mathscr{L}}(\cdot)$. Here, $\mathscr{L}$ is the index of the particular convolutional layer.

$$\mathscr{F}_{\mathscr{L}}(x_i) = \lambda(W_i * x_i + b_i) \tag{1}$$

In the above equation, λ is the rectified linear unit (ReLU) activation function [26]. W_i indicates the i^{th} layer's weights, and b_i denotes the bias.

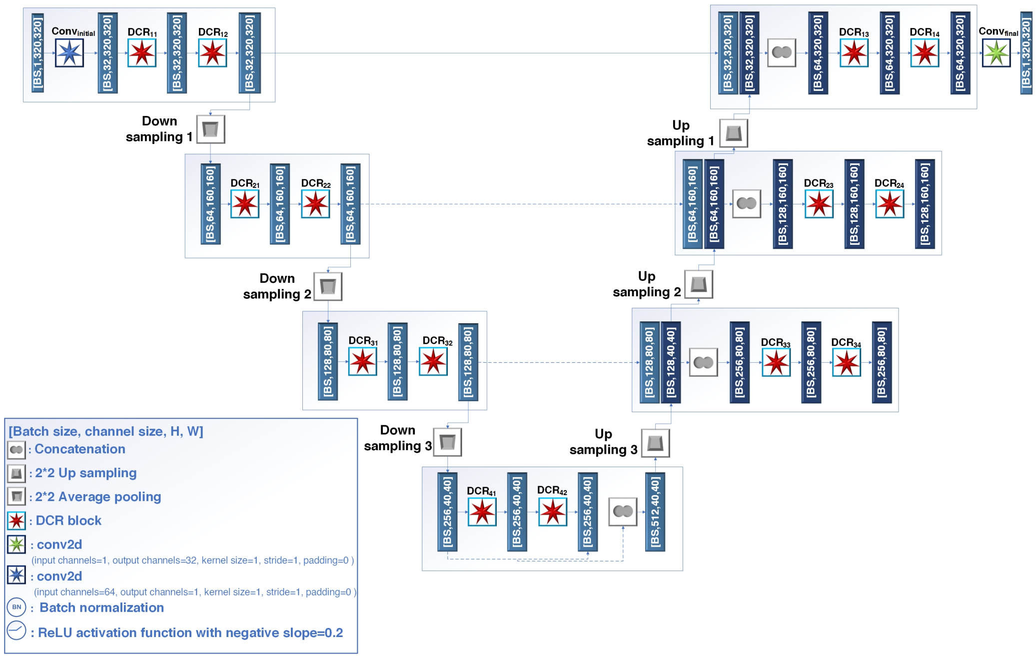

Figure 2: Densely Connected Residual U-Net.

Residual connections [27] add input and output and bypass the mapping function $\mathscr{F}_{\mathscr{L}}(.)$ with a skip connection.

$$x_{\mathscr{L}} = \mathscr{F}_{\mathscr{L}}(x_{\mathscr{L}-1}) + x_{\mathscr{L}-1} \tag{2}$$

The dense connections [20] as shown in Fig. 3 concatenate successive convolutional layers' outputs. Hence, the $\mathscr{L}^{th}$ layer's input will include all the feature maps created by the previous convolutional layers.

$$x_{\mathscr{L}} = \mathscr{F}_{\mathscr{L}}([x_0, x_1, x_2, ..., x_{\mathscr{L}-1}]) \tag{3}$$

The growth rate on the other hand can be defined as follows.

$$\mathscr{K} = k_0 + k \times (\mathscr{L} - 1) \tag{4}$$

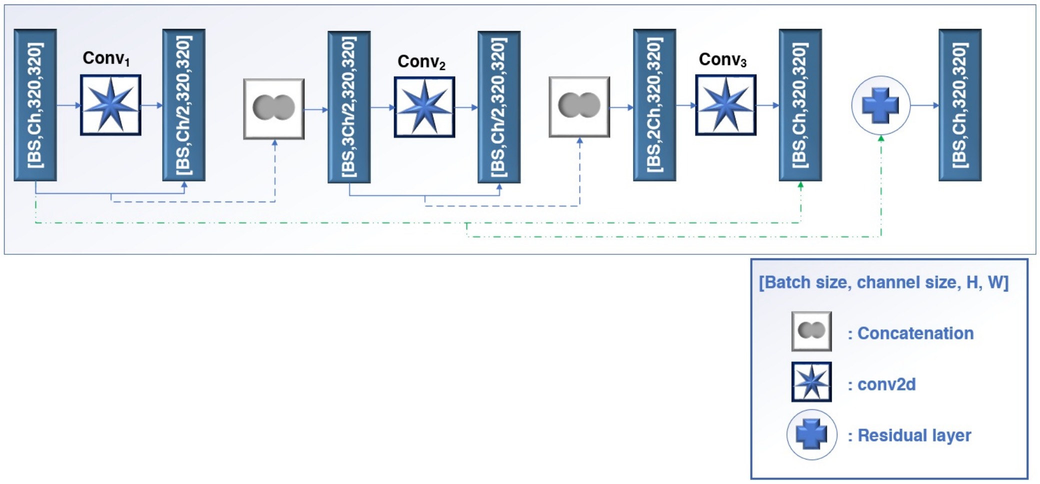

Figure 3: Densely Connected Residual block.

Here, $\mathscr{K}$ is the number of input feature maps to the $\mathscr{L}^{th}$ layer. k is the number of feature maps created by $\mathscr{F}_{\mathscr{L}}$, and k_0 indicates the input channel size.

In MR image data acquisition model, data is undersampled using the following equation.

$$y = \mathscr{F}_{\Omega} x_{orig} \tag{5}$$

Here, y is the undersampled data (observed data) in the k-domain. The $\mathscr{F}_{\Omega}$ operator denotes the undersampled Fourier transform function, and x_{orig} indicates the ground truth image.

2.2. Architecture

In this paper, we have implemented deep learning models for MR image reconstruction by converting two benchmark networks of standard CNN and U-Net into densely connected residual networks. In all of the implementations in this paper, we have normalized ZF images immediately after computing the absolute value of the complex-valued image tensor. To minimize the learning error, for CNN-based structures we applied the Adam optimizer with a weight decay of 10^{-7} and a learning rate of 10^{-4}. In this structure, the β values are set as 0.9 and 0.999. On the other hand, for the U-Net pipeline, the gradient-based optimization technique RMSprop was leveraged with zero weight decay and a 10^{-3} learning rate. In both CNN and U-Net based frameworks we avoided dropout in training, hence we set dropout as zero by default.

2.2.1. CNN based networks

For the standard CNN, we opted for a structure similar to the one that has been used in [19]. We dedicated 5 convolutional layers followed by the ReLU activation functions. Through this configuration, ZF images go through the initial layer with input and output channel sizes 1, and 64 respectively. The next three subsequent layers individually generate 64 feature-map. The final reconstruction layer convolves 64 feature-map into a single channel output. All layers have the same default values for the filter parameters, namely a kernel-size of 3, a stride of 1 and padding size of 1. Then, we modified standard CNN into a densely connected residual CNN by adding DCR Blocks as shown in Fig.1. In this new structure, the initial and final reconstruction layers are the same as the conventional setup without any change. The three central convolutional layers are replaced by 3, 8, and 10 DCR blocks. The DCR block as shown in Fig. 3 contains three convolutional layers that activate by the ReLU function. Inside DCR block, input and generated feature maps of all layers couple with each other and go through the final convolutional layer which generates 64 feature maps. In the last step, input and output feature maps are added together as a residual output [27].

2.2.2. U-Net based networks

In this paper, we have compared two U-Nets with different structures with the proposed DCR U-Net regarding their MR image reconstruction results. Initially, we benefited from the U-Net model that has been introduced in the fastMRI collaborative challenge held jointly by the Facebook AI Research (FAIR) Team and NYU Langone Health [28]. This U-Net framework consists of contracting (or encoding) and expanding (or decoding) parts. Each step of the encoding path contains 2 blocks of 3×3 convolutional layers which downsample the image to half size using the average-pooling method. The decoding part deconvolves and upsamples the image through a 2D transpose convolutional layer. In the decoding path, the input to the deconvolutional blocks couples with feature-map from the same downsampling step. This action prevents a serious reduction in the amount of data. The final step of this U-Net pipeline end with two 1×1 convolutional layers. The final convolutional layer generates the reconstruction image from 16 feature maps after mapping residual learning [27] by adding learned information in output to the input. Then we modified this structure to the one which has been used in [21] as a DensNet for image denoising problem (with fewer parameters to train). In this regard, we added an initial 1×1 convolutional layer that creates 32 feature-maps from one channel ZF image. The activation functions were changed to Parametric Rectified Linear Unit (PReLU). After final expansion, the final layer reconstructs the final image using only one 1×1 convolutional layer with input and output channel sizes of 64 and one, respectively. Contrary to the FAIR U-Net, the encoder path reduces the size of the image up to 40×40 (not 20×20). In this U-Net framework, the downsampling is performed by the max-pooling operation. While the max-pooling function half the size of feature maps by stride 2, the convolutional layer doubles the number of feature maps to hinder feature loss. The up-sampling path double the size of slices using the pixel-shuffle function with upscaling factor of two. So, as the result of using the sub-pixel interpolation method for the upsampling path, the number of feature maps is alleviated to one quarter. Thereafter, this U-Net pipeline was modified to densely connected residual U-Net as shown in Fig. 2. In this proposed structure, the convolutional blocks were replaced by the DCR block. Here, the DCR block again possesses three convolutional layers but these layers are followed by PReLU in contrary to densely connected residual CNN. We set the growth rate of our model to half size of the feature maps.

2.3. Simulation Setting

2.3.1. Dataset

Throughout this study, all models were trained using the fastMRI single-coil dataset [28]. The fastMRI dataset provides a complete and rather recent dataset for MR image reconstruction. This dataset includes both single and multi-coil images. The fastMRI dataset are saved in DICOM, fully sampled k-space data, and reconstructed image formats. There are a total of 1372 single-coil volumes, and the details of these are provided in Table 1.

Each volume contains both k-space domain information and the real image. In this study, the MR data acquisition process was modeled by under-sampling the fully sampled k-space data using the random mask function.

Table 1: fastMRI single-coil dataset configuration [28].

Subset name	Volumes	Slices
Training	973	34742
Validation	199	7135
Test	108	3903
Challenge	92	3305

Then, the training was initiated from created real-valued ZF images. The undersampling is carried out using 8-fold and 4-fold acceleration factors. The target image slices are applied to the simulation settings to calculate the pixel-wise L1 loss between the ground truth and realizations results.

2.3.2. Experimental setup

In this study, MR image reconstruction models were trained using Python 3.6 alongside Pytorch machine-learning package with version 1.4.0. We utilized two GeForce RTX 2080 Ti GPUs with a total memory of 22GB. It was experimentally figured out that 20 epochs would be sufficient for training each of the proposed models. For the baseline realizations (CNN and U-Net) the batch size was set to 16. However, the batch size was reduced as the networks get deeper to be able to fit the data into the available GPUs.

3. Results

3.1. Quantitative results

In this paper, we have performed realization for the two novel DCR based networks in addition to various state-of-the-art MR image reconstruction methodologies from the literature. To evaluate the performance of the networks, Normalized Mean Squared Error (NMSE) [29], Structural Similarity Index Measure (SSIM) [30], and Peak Signal to Noise Ratio (PSNR) [31] indices have been used. The results are reported in Tables 2 and 3, where the methods are ordered with respect to increasing performance. These two tables summarize the simulation results for all the trained networks for both 4-fold and 8-fold acceleration factors. In the preprocessing step, fully-sampled k-space data is undersampled by the random subsampling mask. Afterwards, the data is transformed to the image domain by applying the 2D Inverse Fast Fourier transform (2D-IFFT).

As illustrated in Tables 2 and 3, the addition of DCR blocks leads to promising results and improved MR image reconstruction performance for both U-Net [28] and standard CNN. Appending 10 DCR blocks to the standard CNN improves reconstruction PSNR about 1.25 dB. It can be noticed that as CNN gets deeper by the addition of more DCR blocks, its results improve in all of the performance metrics. The densely connected residual U-Net includes a total of 14 DCR blocks. U-Net with DCR is faster than the DCR-CNN in the testing phase, despite its larger number of network parameters. DCR-CNN performs its computations in all convolutional layers on feature maps of a constant pixel size (320×320) without downsampling them. Hence, this leads to slightly reduced reconstruction speed for the

DCR-CNN when compared with the DCR based U-Net.

Table 2: Simulation results for fastMRI dataset for 4-fold acceleration factor.

Acceleration factor	4-fold				#Parameter	Time (s)
Network	Loss	NMSE (x10-3)	SSIM(x10-3)	PSNR		
ZF	-	41.679	711.59	29.876	-	-
CS-MRI (TV based) [32, 28]	-	36.719±43.5	712.2±224.3	30.846±5.78	-	138.3
CNN [19, 33]	0.308	34. 259±17.43	755. 65±78.76	30.880±2.49	111,744	0.095
k-space DL [9]	0.257	32.060±18.92	763.45±79.35	31.273±2.66	7,756,418	0.173
CNN with 3 DCR blocks	0.298	31.344±17.62	765.97±82.16	31.402 ±2.69	360,960	0.28
KIKI-net [34, 35]	0.291	31.297±17.33	766.52±81.23	31.419±2.78	1,168,128	0.78
CNN with 8 DCR blocks	0.287	28.426±18.09	778.68±84.93	32.038±2.98	960,640	0.73
CNN with 10 DCR blocks	0.286	28.042±18.15	780.73±85.04	32.133±3.03	1,200,512	0.92
Deep Cascade CNN [19, 33]	0.280	26.520±18.61	790.00±85.15	32.412±3.14	111,744	0.417
fastMRI U-Net [28, 35]	0.281	26.821±18.18	785.93±86.16	32.419±3.171	7,756,097	0.154
Modified U-Net	0.282	26.637±18.25	784.77±85.28	32.466±3.172	6,618,597	0.45
U-Net with DCR	0.279	25.961±18.20	790.14±86.15	32.651±3.271	10,516,083	0.79

Table 3: Simulation results for fastMRI dataset for 8-fold acceleration factor.

Acceleration			8-fold		#Parameter	Time (s)
Network	Loss	NMSE (x10-3)	SSIM(x10-3)	PSNR		
ZF	-	77.751	603.37	26.921	-	-
CS-MRI (TV based) [32, 28]	-	71.921±44.66	608.9±242.2	27.351±4.133	-	134.65
CNN [19, 33]	0.451	69.277±19.88	637.76±100.66	27.462±2.01	111,744	0.096
CNN with 3 DCR blocks	0.433	62.360±19.59	650.92±104.83	27.953±2.08	360,960	0.28
KIKI-net [34, 35]	0.431	62.103±19.41	644.20±103.54	28.020±2.11	1,168,128	0.78
k-space DL [9]	0.437	58.376±21.89	651.80±103.98	28.292±2.07	7,756,418	0.174
CNN with 8 DCR blocks	0.406	52.318±21.54	670.19±112.73	28.857±2.22	960,640	0.73
CNN with 10 DCR blocks	0.402	50.766±21.94	672.01±115.39	29.026±2.28	1,200,512	0.92
Deep Cascade CNN [19, 33]	0.417	54.827±23.25	654.92±113.77	28.639±2.24	111,744	0.418
fastMRI U-Net [28, 35]	0.380	43.275±23.47	692.96±118.22	29.952±2.55	7,756,097	0.154
Modified U-Net	0.381	43.234±23.36	691.95±117.12	29.950±2.55	6,618,597	0.506
U-Net with DCR	0.376	41.605±23.67	699.77±117.36	30.198±6.51	10,516,083	0.8

The testing error loss curves are presented in Figs. 4(a) and 4(b). In general, this curve gives an idea of how well the model is generalizing through the validation/testing steps. As we can see, the loss value decreases with the increasing number of epochs and converges to a stable point. Moreover, the application of DCR blocks significantly reduced the resulting loss amplitude, when compared to the structures which lack the DCR blocks.

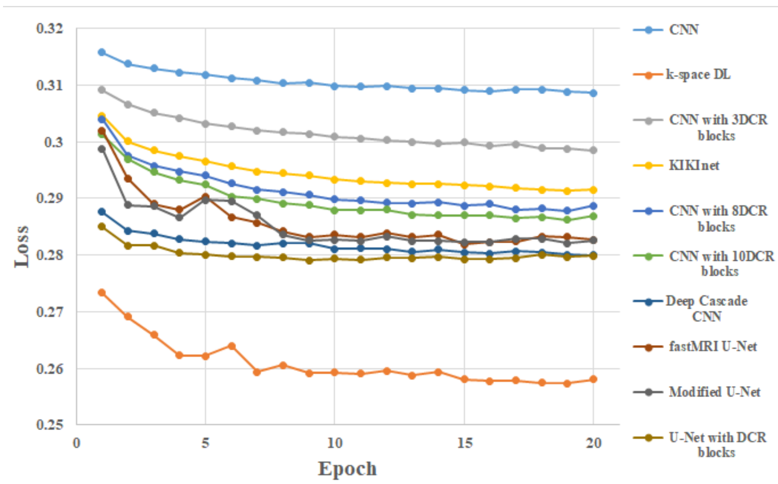

(a)

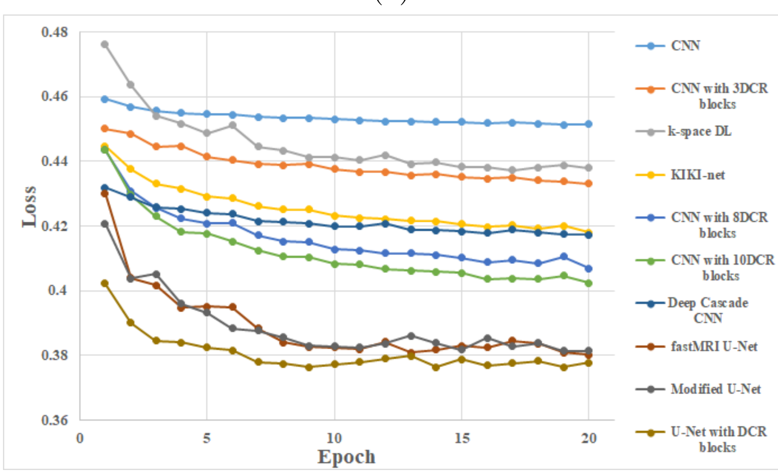

(b)

Figure 4: Testing phase loss curves depending on the epochs; (a) undersampled data with 4-fold acceleration factor (b) undersampled data with an 8-fold acceleration factor.

In Fig. 5, run time versus PSNR values are given for both the developed networks and also the networks used for comparison. The given time values indicate the time needed for reconstructing 32 slices in the testing phase. It can be concluded that all these frameworks with noticeable reconstruction results can get realized in a real-time setting. It can also be seen that the results given for the 4-fold and 8-fold settings complement each other naturally.

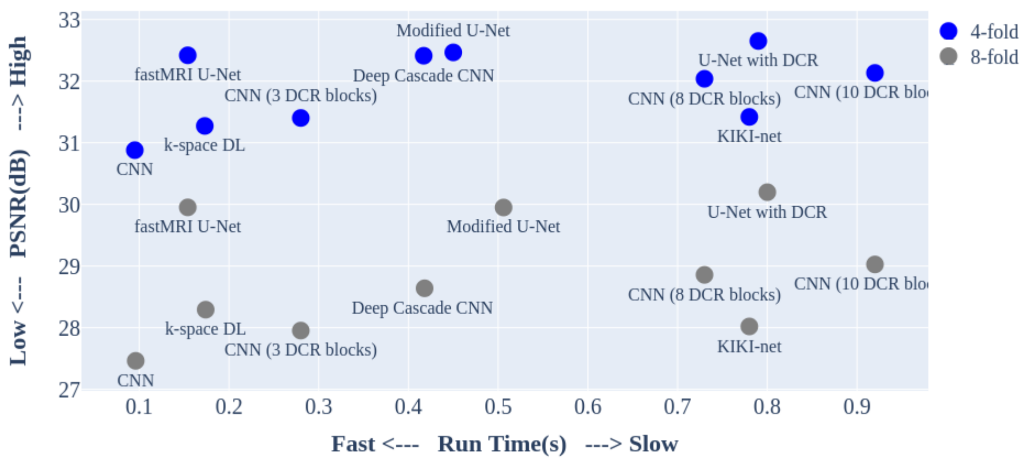

Figure 5: The run time vs. PSNR value of different models.

The acquired quantitative results have been evaluated using statistical assessment tests. To do so, one-way analysis of variance (ANOVA) tests and paired t-tests were applied to verify statistically significant differences among developed networks and their related assessment metrics. These two tests can prove that the acquired reconstruction results are attributed to a specific cause and they are not provided by chance or randomly. In this evaluation, threshold p-values are set to α=0.05. For the proposed pipelines, the paired

t-tests ended up with the overwhelming suggestion of 95% confidence (p-values ≤ 0.05). The ANOVA test results reported more than 99% confidence by indicating p-values ≤ 0.01 for all the proposed methods, in all different settings including different assessment metrics and acceleration factors.

In addition to the benchmark fastMRI dataset, we have tested our trained models using yet another comparatively common dataset, namely the IXI dataset (https://brain-development.org/ixi-dataset/) [14, 36]. This dataset contains around 615 lateral brain MR image volumes. Each volume includes 150 real-valued slices of the size 256×256. The results for the IXI dataset are summarized in Tables 4 and 5. These results indicate that, the proposed novel models can reconstruct MR images from different parts of the body without the need for retraining.

Table 4: Simulation results for IXI dataset for 4-fold acceleration factor.

Acceleration factor	4-fold				#Parameter	Time (s)
Network	Loss	NMSE (x10-3)	SSIM(x10-3)	PSNR		
ZF	-	50.427	727.39	28.078	-	-
CNN [19, 33]	0.189	39.281±4.79	751.86±37.03	29.164±1.64	111,744	0.220
k-space DL [9]	0.122	38.011±6.38	758.72±39.62	29.454±1.73	7,756,418	0.485
CNN with 3 DCR blocks	0.181	35.935±4.43	762.43±36.00	29.554±1.66	360,960	0.393
KIKI-net [34, 35]	0.174	36.440±5.68	777.40±34.07	29.513±1.70	1,168,128	0.504
CNN with 8 DCR blocks	0.166	31.100±3.58	791.20±29.13	30.176±1.62	960,640	0.416
CNN with 10 DCR blocks	0.165	30.474±3.48	792.65±29.69	30.263±1.62	1,200,512	0.546
Deep Cascade CNN [19, 33]	0.164	29.814±4.35	801.91±25.82	30.365±1.73	111,744	0.325
fastMRI U-Net[28, 35]	0.162	29.232±3.17	802.21±33.38	30.445±1.61	7,756,097	0.15
Modified U-Net	0.168	30.056±3.17	801.79±39.44	30.320±1.59	6,618,597	0.502
U-Net with DCR	0.164	28.287±3.09	806.03±38.27	30.586±1.59	10,516,083	0.505

Table 5: Simulation results for IXI dataset for 8-fold acceleration factor.

Acceleration factor	8-fold				#Parameter	Time (s)
Network	Loss	NMSE (x10-3)	SSIM(x10-3)	PSNR		
ZF	-	97.763	632.04	25.211	-	-
CNN [19, 33]	0.296	90.867±13.20	636.31±50.29	25.523±1.80	111,744	0.221
CNN with 3 DCR blocks	0.283	85.317±11.49	654.08±48.94	25.791±1.76	360,960	0.393
k-space DL [9]	0.295	88.09±14.28	640.11±52.95	25.601±1.81	7,756,418	0.481
KIKI-net [34, 35]	0.28	83.825±10.66	663.46±54.12	25.868±1.72	1,168,128	0.504
CNN with 8 DCR blocks	0.271	82.235±10.17	680.08±43.45	25.943±1.67	960,640	0.477
CNN with 10 DCR blocks	0.266	78.691±10.03	680.87±43.31	26.136±1.67	1,200,512	0.55
Deep Cascade CNN [19, 33]	0.262	73.726±11.33	689.13±42.32	26.335±1.74	111,744	0.327
fastMRI U-Net [28, 35]	0.263	77.472±10.05	684.72±47.74	26.209±1.69	7,756,097	0.15
Modified U-Net	0.273	76.996±10.09	684.79±51.37	26.237±1.70	6,618,597	0.502
U-Net with DCR	0.261	71.911±8.64	696.49±46.59	26.529±1.63	10,516,083	0.505

3.2. Qualitative results

In this study, also a fair qualitative comparison was performed between reconstructed images by 2 state-of-the-art deep learning models and their densely connected residual form. Figs. 6 and 7 display the real image, ZF image, Region of Interest (ROI) and error map for images reconstructed by these frameworks. Fig. 6 provides the resulting images for undersampled data with 4-fold acceleration factor, whereas Fig. 7 is for undersampled data with 8-fold acceleration factor. As we expected from Tables 2 and 3, these figures show that the densely connected residual models restore more detail and pattern whereas the conventional methods reconstructed blurred images.

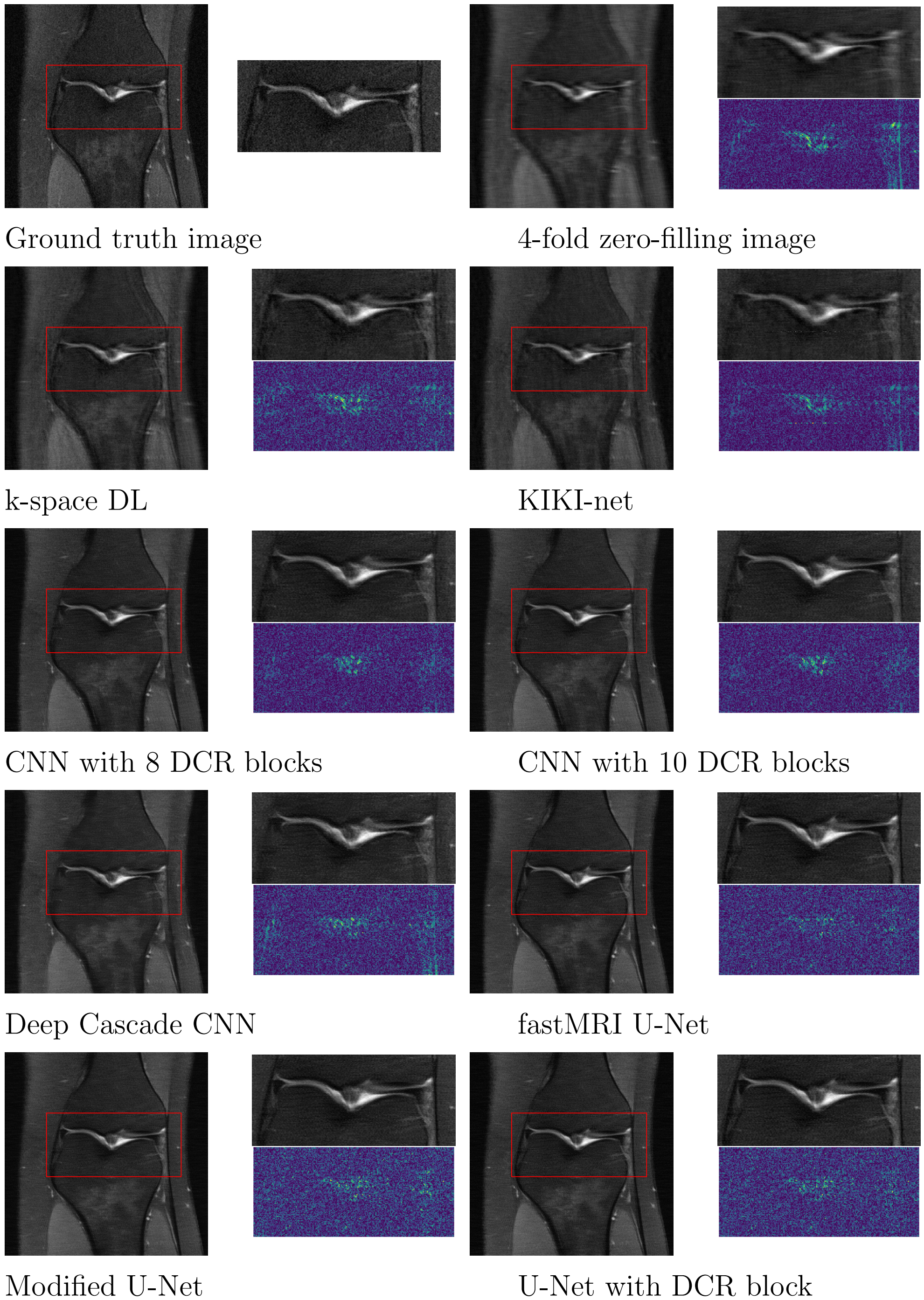

Figure 6: Developed model's reconstruction results, ROI, and error map for 4-fold undersampled data.

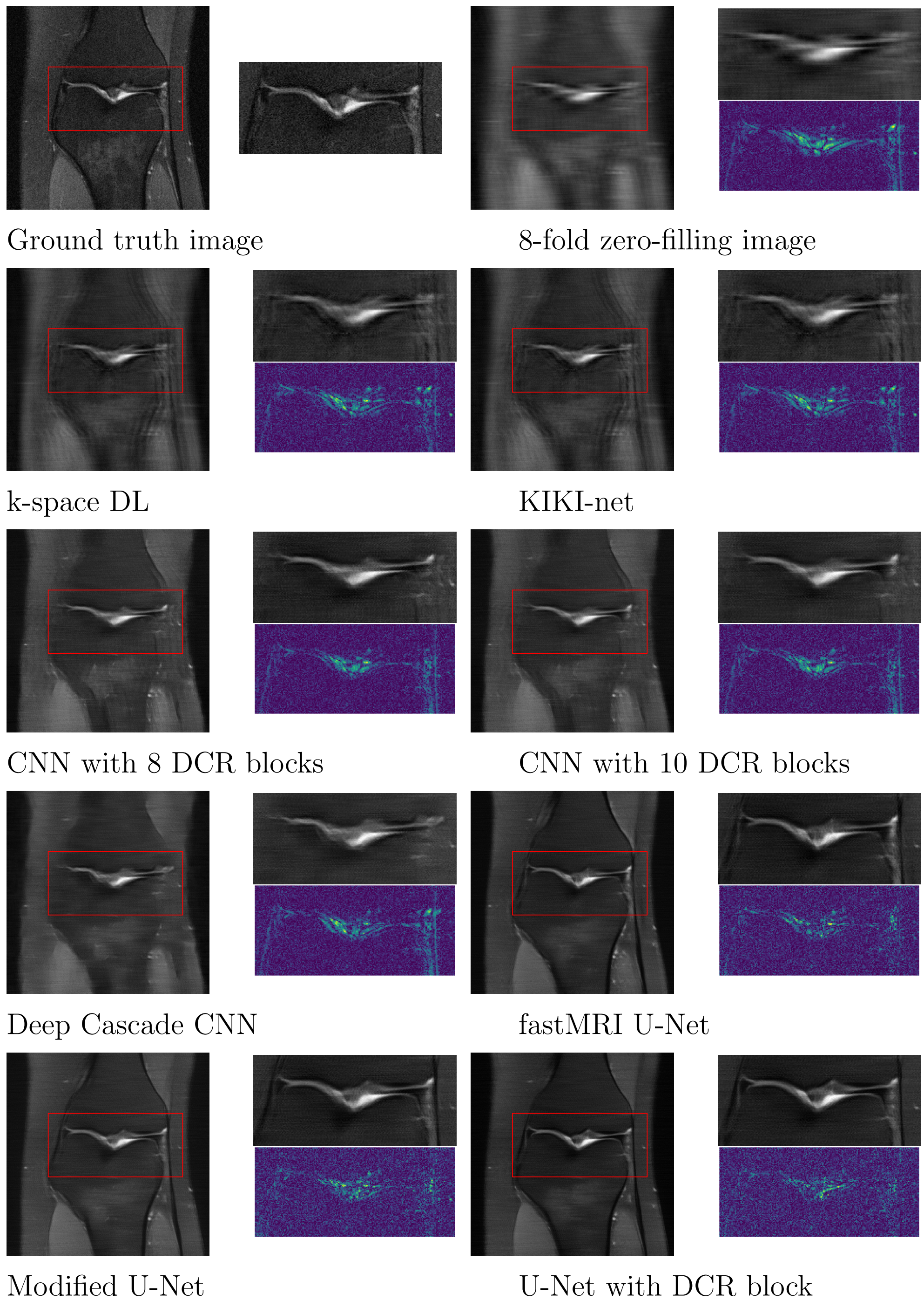

Figure 7: Developed model's reconstruction results, ROI, and error map for 8-fold under-sampled data.

As discussed in the introduction section of this paper, the major goal of MR image reconstruction based on deep learning is to speed up MR image reconstruction. To do so, we need to decrease signal acquisition time without significantly reducing image quality. In this regard, more aggressive undersampling with larger acceleration factors are also performed. Deep learning-based advanced methodologies are very effective in fast and high-quality image reconstruction from this reduced acquired data.

In this paper, we have trained the deep models by using ZF images as inputs. For the undersampling of k-space data 4-fold and 8-fold acceleration factors have been used. The below table summarizes the PSNR improvements of the reconstructed images when compared to the initial ZF estimate for both 4-fold and 8-fold undersampling cases.

Table 6: Reconstructed image's PSNR improvement compared to the ZF image.

Network	Acceleration factor	
	4-fold	8-fold
PSNR difference (CNN - ZF)	1.004	0.541
PSNR difference (CNN with 10 DCR blocks - ZF)	2.257	2.105
PSNR difference (U-Net with DCR bloks – ZF)	2.775	3.277

The results in Table 6 indicate that the proposed networks are capable to reconstruct high-quality images even with the more aggressive undersampling rates. For both 4-fold and 8-fold undersampling, the proposed frameworks result in significantly better images compared to the ZF estimates.

4. Conclusion

Recently, dense connections have shown their efficiency in different image processing problems for preventing the vanishing gradient problem in deep learning-based solutions. Motivated by this successful application of dense connections in a variety of problems, here we proposed an MR image reconstruction pipeline that includes a residual densely connected structure. The quantitative and qualitative results are summarized for images reconstructed from undersampled data with 4-fold and 8-fold acceleration factors. By coupling the DCR blocks into two state-of-the-art deep learning frameworks, promising simulation results have been obtained. The MR image reconstruction results indicate improved performance when compared to the original structures lacking dense connections. The results again imply that DCR blocks provide a possible solution for further deepening of MR reconstruction network structures, without the information loss problem which is usually associated with increased depth. The results showcase that increasing the number of DCR blocks, translates into improved reconstruction performance. These results are observed in both cases when CNN-based and U-Net based networks are augmented with DCR blocks. The PSNR results for densely connected CNN structure with 10 DCR blocks are improved significantly in comparison to the plain CNN, where the improvement lies around 1.25 - 1.56 dB. Moreover, statistical evaluation tests were realized, and the statistical significance of the improved results was verified. In conclusion, the introduced novel use of dense connections in the form of DCR blocks has shown great potential for possible use in MRI reconstruction deep models.

Conflict of interest statement

None of the authors have any conflicts to declare, financial or otherwise.

Acknowledgment

This work has been sponsored by TUBITAK (The Scientific and Technological Research Council of Turkey) under project no. 119E248.

References

[1] Y. Jin, G. Yang, Y. Fang, R. Li, X. Xu, Y. Liu, X. Lai, 3D PBV-Net: an automated prostate MRI data segmentation method, Computers in Biology and Medicine 128 (2021) 104160.

[2] M. Lustig, D. L. Donoho, J. M. Santos, J. M. Pauly, Compressed sensing MRI, IEEE Signal Processing Magazine 25 (2) (2008) 72–82. doi:10.1109/MSP.2007.914728.

[3] A. K. Tanc, E. M. Eksioglu, MRI reconstruction with joint global regularization and transform learning, Computerized Medical Imaging and Graphics 53 (2016) 1–8. doi:10.1016/j.compmedimag.2016.06.004.

[4] D. Zhang, J. He, Y. Zhao, M. Du, MR image super-resolution reconstruction using sparse representation, nonlocal similarity and sparse derivative prior, Computers in Biology and Medicine 58 (2015) 130–145. doi:10.1016/j.compbiomed.2014.12.023.

[5] R. Ahmad, C. A. Bouman, G. T. Buzzard, S. Chan, S. Liu, E. T. Reehorst, P. Schniter, Plug-and-play methods for magnetic resonance

imaging: Using denoisers for image recovery, IEEE Signal Processing Magazine 37 (1) (2020) 105–116. doi:10.1109/MSP.2019.2949470.

[6] E. M. Eksioglu, Decoupled algorithm for MRI reconstruction using nonlocal block matching model: BM3D-MRI, Journal of Mathematical Imaging and Vision 56 (3) (2016) 430–440.

[7] E. M. Eksioglu, A. K. Tanc, Denoising AMP for MRI reconstruction: BM3D-AMP-MRI, SIAM Journal on Imaging Sciences 11 (3) (2018) 2090–2109. doi:10.1137/18M1169655.

[8] S. Wang, Z. Su, L. Ying, X. Peng, S. Zhu, F. Liang, D. Feng, D. Liang, Accelerating magnetic resonance imaging via deep learning, in: 2016 IEEE 13th International Symposium on Biomedical Imaging (ISBI), IEEE, 2016, pp. 514–517.

[9] Y. Han, L. Sunwoo, J. C. Ye, k-space deep learning for accelerated MRI, IEEE Transactions on Medical Imaging 39 (2) (2019) 377–386. doi:10.1109/TMI.2019.2927101.

[10] D. Lee, J. Yoo, S. Tak, J. C. Ye, Deep residual learning for accelerated MRI using magnitude and phase networks, IEEE Transactions on Biomedical Engineering 65 (9) (2018) 1985–1995. doi:10.1109/TBME.2018.2821699.

[11] B. Zhu, J. Z. Liu, S. F. Cauley, B. R. Rosen, M. S. Rosen, Image reconstruction by domain-transform manifold learning, Nature 555 (7697) (2018) 487–492.

[12] K. Hammernik, T. Klatzer, E. Kobler, M. P. Recht, D. K. Sodickson, T. Pock, F. Knoll, Learning a variational network for reconstruction of accelerated MRI data, Magnetic Resonance in Medicine 79 (6) (2018) 3055–3071.

[13] O. Ronneberger, P. Fischer, T. Brox, U-Net: Convolutional networks for biomedical image segmentation, in: Medical Image Computing and Computer-Assisted Intervention – MICCAI 2015, Springer, Springer International Publishing, 2015, pp. 234–241.

[14] I. Njeh, H. Mzoughi, M. B. Slima, A. B. Hamida, C. Mhiri, K. B. Mahfoudh, Deep convolutional encoder-decoder algorithm for MRI brain reconstruction, Medical & Biological Engineering & Computing (2020) 1–22.

[15] A. Falvo, D. Comminiello, S. Scardapane, M. Scarpiniti, A. Uncini, A wide multimodal dense U-Net for fast magnetic resonance imaging, in: 2020 28th European Signal Processing Conference (EUSIPCO), IEEE, 2021, pp. 1274–1278. doi:10.23919/Eusipco47968.2020.9287519.

[16] D. Lee, J. Yoo, J. C. Ye, Deep residual learning for compressed sensing MRI, in: 2017 IEEE 14th International Symposium on Biomedical Imaging (ISBI 2017), IEEE, 2017, pp. 15–18.

[17] C. M. Hyun, H. P. Kim, S. M. Lee, S. Lee, J. K. Seo, Deep learning for undersampled MRI reconstruction, Physics in Medicine & Biology 63 (13) (2018) 135007.

[18] S. Hochreiter, The vanishing gradient problem during learning recurrent neural nets and problem solutions, International Journal of Uncertainty, Fuzziness and Knowledge-Based Systems 06 (02) (1998) 107–116.

[19] J. Schlemper, J. Caballero, J. V. Hajnal, A. N. Price, D. Rueckert, A deep cascade of convolutional neural networks for dynamic MR image reconstruction, IEEE Transactions on Medical Imaging 37 (2) (2017) 491–503. doi:10.1109/TMI.2017.2760978.

[20] G. Huang, Z. Liu, L. Van Der Maaten, K. Q. Weinberger, Densely connected convolutional networks, in: Proceedings of the IEEE conference on Computer Vision and Pattern Recognition, 2017, pp. 4700–4708.

[21] B. Park, S. Yu, J. Jeong, Densely connected hierarchical network for image denoising, in: Proceedings of the IEEE/CVF Conference on Computer Vision and Pattern Recognition Workshops, 2019, pp. 0–0.

[22] Y. Zhang, Y. Tian, Y. Kong, B. Zhong, Y. Fu, Residual dense network for image restoration, IEEE Transactions on Pattern Analysis and Machine Intelligence (2020) 1–1doi:10.1109/TPAMI.2020.2968521.

[23] Y. Yuan, W. Qin, X. Guo, M. Buyyounouski, S. Hancock, B. Han, L. Xing, Prostate segmentation with encoder-decoder densely connected convolutional network (Ed-Densenet), in: 2019 IEEE 16th International Symposium on Biomedical Imaging (ISBI 2019), 2019, pp. 434–437. doi:10.1109/ISBI.2019.8759498.

[24] J. Du, L. Wang, A. Gholipour, Z. He, Y. Jia, Accelerated super-resolution mr image reconstruction via a 3D densely connected deep

convolutional neural network, in: 2018 IEEE International Conference on Bioinformatics and Biomedicine (BIBM), 2018, pp. 349–355. doi:10.1109/BIBM.2018.8621073.

[25] Y. Chen, Y. Xie, Z. Zhou, F. Shi, A. G. Christodoulou, D. Li, Brain MRI super resolution using 3D deep densely connected neural networks, in: 2018 IEEE 15th International Symposium on Biomedical Imaging (ISBI 2018), 2018, pp. 739–742. doi:10.1109/ISBI.2018.8363679.

[26] V. Nair, G. E. Hinton, Rectified linear units improve restricted boltzmann machines, in: Proceedings of the 27th International Conference on International Conference on Machine Learning, ICML'10, 2010, p. 807–814.

[27] K. He, X. Zhang, S. Ren, J. Sun, Deep residual learning for image recognition, in: Proceedings of the IEEE conference on computer vision and pattern recognition, 2016, pp. 770–778.

[28] J. Zbontar, F. Knoll, A. Sriram, M. J. Muckley, M. Bruno, A. Defazio, M. Parente, K. J. Geras, J. Katsnelson, H. Chandarana, et al., fastMRI: An open dataset and benchmarks for accelerated MRI, arXiv preprint arXiv:1811.08839 (2018).

[29] P. Händel, Understanding normalized mean squared error in power amplifier linearization, IEEE Microwave and Wireless Components Letters 28 (11) (2018) 1047–1049. doi:10.1109/LMWC.2018.2869299.

[30] Zhou Wang, A. C. Bovik, H. R. Sheikh, E. P. Simoncelli, Image quality assessment: from error visibility to structural similarity, IEEE Transac-

tions on Image Processing 13 (4) (2004) 600–612. doi:10.1109/TIP.2003.819861.

[31] A. Horé, D. Ziou, Is there a relationship between peak-signal-to-noise ratio and structural similarity index measure?, IET Image Processing 7 (1) (2013) 12–24.

[32] M. Uecker, P. Lai, M. J. Murphy, P. Virtue, M. Elad, J. M. Pauly, S. S. Vasanawala, M. Lustig, ESPIRiT—an eigenvalue approach to autocalibrating parallel MRI: Where SENSE meets GRAPPA, Magnetic Resonance in Medicine 71 (3) (2014) 990–1001. doi:10.1002/mrm.24751.

[33] J. Schlemper, J. Caballero, J. V. Hajnal, A. Price, D. Rueckert, A deep cascade of convolutional neural networks for MR image reconstruction, in: International Conference on Information Processing in Medical Imaging, Springer, 2017, pp. 647–658.

[34] T. Eo, Y. Jun, T. Kim, J. Jang, H.-J. Lee, D. Hwang, KIKI-net: cross-domain convolutional neural networks for reconstructing undersampled magnetic resonance images, Magnetic Resonance in Medicine 80 (5) (2018) 2188–2201.

[35] Z. Ramzi, P. Ciuciu, J.-L. Starck, Benchmarking deep nets MRI reconstruction models on the fastMRI publicly available dataset, in: 2020 IEEE 17th International Symposium on Biomedical Imaging (ISBI), IEEE, 2020, pp. 1441–1445.

[36] D. Kocanaogullari and E. M. Eksioglu, Deep learning for MRI reconstruction using a novel projection based cascaded network, in: 2019

IEEE 29th International Workshop on Machine Learning for Signal Processing (MLSP), 2019. doi:10.1109/MLSP.2019.8918715.